An integrated single-cell RNA-seq atlas of the mouse hypothalamic paraventricular nucleus links transcriptomic and functional types

Berkhout, J. B.; Poormoghadam, D.; Yi, C.; Kalsbeek, A.; Meijer, O. C.; Mahfouz, A.

DOI
10.1111/jne.13367

Publication date
2024

Document Version
Final published version

Published in
Journal of Neuroendocrinology

Citation (APA)
Berkhout, J. B., Poormoghadam, D., Yi, C., Kalsbeek, A., Meijer, O. C., & Mahfouz, A. (2024). An integrated single-cell RNA-seq atlas of the mouse hypothalamic paraventricular nucleus links transcriptomic and functional types. *Journal of Neuroendocrinology*, *36*(2), Article e13367. https://doi.org/10.1111/jne.13367

Received: 19 July 2023 | Revised: 30 November 2023 | Accepted: 30 December 2023

DOI: 10.1111/jne.13367

ORIGINAL ARTICLE

Journal of Neuroendocrinology WILEY

An integrated single-cell RNA-seq atlas of the mouse hypothalamic paraventricular nucleus links transcriptomic and functional types

J. B. Berkhout[1,2] | D. Poormoghadam[3,4] | C. Yi[3,5] | A. Kalsbeek[3,4,5] | O. C. Meijer[1] | A. Mahfouz[2,6]

[1]Division of Endocrinology, Department of Medicine, Leiden University Medical Centre, Leiden, The Netherlands

[2]Department of Human Genetics, Leiden University Medical Centre, Leiden, The Netherlands

[3]Laboratory of Endocrinology, Department of Laboratory Medicine, Amsterdam UMC, University of Amsterdam, Amsterdam, The Netherlands

[4]Netherlands Institute for Neuroscience, Amsterdam, The Netherlands

[5]Department of Endocrinology and Metabolism, Amsterdam University Medical Centers, Amsterdam, The Netherlands

[6]Division of Pattern Recognition and Bioinformatics, Department of Intelligent Systems, Technical University Delft, Delft, The Netherlands

Correspondence
J. B. Berkhout, Division of Endocrinology, Department of Medicine, Leiden University Medical Centre, Leiden, The Netherlands.
Email: j.b.berkhout@lumc.nl

Funding information
ZonMw, Grant/Award Number: 09120012010051

Abstract

The hypothalamic paraventricular nucleus (PVN) is a highly complex brain region that is crucial for homeostatic regulation through neuroendocrine signaling, outflow of the autonomic nervous system, and projections to other brain areas. In the past years, single-cell datasets of the hypothalamus have contributed immensely to the current understanding of the diverse hypothalamic cellular composition. While the PVN has been adequately classified functionally, its molecular classification is currently still insufficient. To address this, we created a detailed atlas of PVN transcriptomic cell types by integrating various PVN single-cell datasets into a recently published hypothalamus single-cell transcriptome atlas. Furthermore, we functionally profiled transcriptomic cell types, based on relevant literature, existing retrograde tracing data, and existing single-cell data of a PVN-projection target region. Finally, we validated our findings with immunofluorescent stainings. In our PVN atlas dataset, we identify the well-known different neuropeptide types, each composed of multiple novel subtypes. We identify *Avp-Tac1*, *Avp-Th*, *Oxt-Foxp1*, *Crh-Nr3c1*, and *Trh-Nfib* as the most important neuroendocrine subtypes based on markers described in literature. To characterize the preautonomic functional population, we integrated a single-cell retrograde tracing study of spinally projecting preautonomic neurons into our PVN atlas. We identify these (presympathetic) neurons to cocluster with the *Adarb2*$^{+}$ clusters in our dataset. Further, we identify the expression of receptors for *Crh*, *Oxt*, *Penk*, *Sst*, and *Trh* in the dorsal motor nucleus of the vagus, a key region that the pre-

J. B. Berkhout, and D. Poormoghadam contributed equally as shared first authors.

O. C. Meijer, and A. Mahfouz contributed equally as shared last author.

parasympathetic PVN neurons project to. Finally, we identify *Trh-Ucn3* and *Brs3-Adarb2* as some centrally projecting populations. In conclusion, our study presents a detailed overview of the transcriptomic cell types of the murine PVN and provides a first attempt to resolve functionality for the identified populations.

KEYWORDS
hypothalamus, neuroendocrine, paraventricular, preautonomic, single-cell

1 | INTRODUCTION

The hypothalamus is a highly complex brain region that is crucial for homeostatic regulation. It consists of several nuclei that are functionally and molecularly diverse. Single-cell RNA sequencing has contributed immensely to the current understanding of the cellular composition of the hypothalamus. A recently published single-cell atlas based on 17 single-cell datasets currently provides the most high-resolution insight into the cellular makeup of the murine hypothalamus.[1] Yet, not all hypothalamic nuclei are represented at equal resolution in this atlas.

One of the underrepresented nuclei is the paraventricular nucleus (PVN), a small nucleus of the anterior hypothalamus, adjacent to the third ventricle. It is composed of several neuropeptidergic neuron types, mainly expressing arginine-vasopressin (AVP), oxytocin (OXT), corticotropin-releasing hormone (CRH), thyrotropin-releasing hormone (TRH), and somatostatin (SST).[2] These are involved in various homeostatic processes, including the regulation of hormonal axes through neuroendocrine neurons, regulation of the autonomic nervous system through preautonomic neurons, and regulation of—inter alia—behavior through centrally projecting neurons.[2–5]

The neuroendocrine subset of neurons is usually described as being subdivided into the large magnocellular and smaller parvocellular neurons projecting to either the posterior pituitary or the median eminence. The magnocellular neurons release the neurohormones AVP and OXT into the systemic bloodstream via the posterior pituitary, whereas parvocellular neurons release CRH, TRH, and SST in the median eminence to be transported to the anterior pituitary via the hypophyseal portal system. In the anterior pituitary, CRH/AVP, TRH, and SST act on the different populations of trophic cells to stimulate or inhibit the hypothalamus–pituitary–adrenal (HPA), hypothalamus–pituitary–thyroid, and hypothalamus–pituitary–somatic (HPS) axes, respectively.

The preautonomic neurons project to the sympathetic and parasympathetic preganglionic neurons in the intermediolateral nucleus (IML) of the spinal cord and dorsal motor nucleus of the vagus (DMV) in the brainstem, respectively. In addition, these preautonomic neurons project to other brainstem nuclei such as the nucleus of the solitary tract, the central gray, and the raphe nucleus.[2] Though the existence of these projections has been described, the molecular identity of these neurons has not been completely elucidated yet. Several studies have attempted to uncover the molecular identity of the preautonomic neurons in the PVN, by utilizing retrograde tracing in combination with immunohistochemistry or in situ hybridization.[2,6–8] These studies have revealed the expression of several neuropeptides, like AVP, OXT, enkephalin (PENK), and dynorphin (PDYN) in these neurons. However, these studies were only able to characterize roughly half of retrogradely traced neurons, thus necessitating further characterization of the neuropeptides and other markers involved.

Neuropeptidergic projections to other central locations upstream of the brainstem exist as well and are often associated with behavioral modulation. For instance, magnocellular Oxt^{+} neurons were reported to project to the amygdala,[9] and parvocellular Oxt^{+} neurons were reported to project to the nucleus of the solitary tract and nucleus accumbens.[5,9] Both magnocellular and parvocellular Oxt^{+} neurons were also reported to project to the ventral tegmental area.[10] Further literature on oxytocinergic central connections has been extensively reviewed by Grinevich and Neumann.[11] Similarly, the central projections and function of Avp^{+} neurons have been reported extensively.[12] For other neuropeptides, like SST and TRH, the literature on central projections is unfortunately less extensive.

While the PVN has been adequately classified functionally (Figure 1A), the molecular classification is currently insufficient. Even less well-described is the relation between the molecular and functional classifications. For instance, it is not known whether the centrally projecting neurons are a separate population of PVN neurons or a subset of the neuroendocrine and/or preautonomic neurons. This lack of insight in the complexity of this region is impeding research progress, since targeting a single functional pathway is difficult without knowledge of the transcriptomic identity of the different functional types. To address this issue, we aimed to create a comprehensive atlas of PVN transcriptomic types from existing scRNA-seq datasets. Furthermore, we aimed to associate transcriptomic and functional types based on literature of neuroendocrine neuron-enriched genes, existing retrograde tracing data, and a single-cell dataset of a PVN-projection target region.

2 | RESULTS

2.1 | PVN neuropeptidergic neurons consist of multiple subpopulations

To create the PVN atlas, we supplemented the whole-hypothalamus atlas[1] with various PVN and neuropeptide-specific single-cell datasets that were originally not included in the atlas.[5,13–16] These datasets

were integrated using scANVI,[17] an integration method derived from scVI,[18] the method used for the original HypoMap integration. From the integrated dataset, PVN neurons were selected, and the resulting subset was clustered. Finally, the identified clusters were annotated based on enriched genes (Figure 1B).

After integration and annotation of the dataset, we first validated the integration by visually inspecting the intermixing of datasets in the dimensionality reduction plot (Figure S1A). Then, we set out to characterize the neuronal populations and subpopulations. All expected major neuropeptidergic neuron populations were found (Figure 1C,D), as well as some nonneuropeptidergic populations. Three populations in the dataset were excluded based on in situ expression data: *Tcf7l2-Shox2*, *Slc32a1-Dlx1*, and *Trh-Zic1* neurons (Figure S2A). Anatomically, markers for these populations are found primarily in the thalamus and/or subparaventricular zone, especially compared with the rare immunoreactive neurons within the PVN (Figure S2B–D). Thus, the relevance of these neurons for PVN function is unclear, given the low frequency of occurrence in the PVN and their high abundance in bordering regions. All remaining clusters were positive for the vesicular glutamate transporter gene *Slc17a6* and overall lacked the vesicular GABA transporter gene *Slc32a1* (Figure S1B). A rare *Slc32a1*$^+$ population has been described in the PVN,[19] raising the question if this population could be reproduced in the atlas. Although sparse *Slc32a1* expression can be observed in the atlas, it is unclear if this is of biological relevance, as these neurons did not form distinct *Slc32a1*$^+$ (sub)clusters within the atlas taxonomy. Interestingly, despite the lack of *Slc32a1*, some of the neurons were positive for GABA biosynthesis enzymes, in particular for *Gad2* (Figure S1B).

The identified clusters were annotated as neuropeptidergic subtypes, except the *Asb4-Adarb2*, *Brs3-Adarb2*, and *Slc17a6-Adarb2* populations, which were not annotated as neuropeptidergic because of relatively low neuropeptide expression levels. Neuropeptidergic populations were further divided into subpopulations based on secondary markers.

The *Avp*$^+$ and *Oxt*$^+$ neurons were found to often present some level of coexpression of both genes (Figure 1D), despite this being rarely observed at protein level.[20] These clusters were characterized as either *Avp*$^+$ or *Oxt*$^+$, based on which of the two genes was most abundantly expressed. This yielded *Avp-Adarb2*, *Avp-Tac1*, *Avp-Th*, *Oxt-Foxp1*, and *Oxt-Adarb2* as the subpopulations of *Avp*$^+$ and *Oxt*$^+$ neurons (Figure 1D). We further identified one population of *Penk*$^+$ neurons, *Penk-Adarb2*; two subpopulations of *Crh*$^+$ neurons, *Crh-Nr3c1* and *Crh-Adarb2*; two subpopulations of *Sst*$^+$ neurons, *Sst-Calb2* and *Sst-Sfrp2*; and two subpopulations of *Ghrh*$^+$ neurons, *Ghrh-Adarb2* and *Trh-Ghrh* (Figure 1D).

Finally, the *Trh*$^+$ neurons were split in multiple categories: *Trh-Ghrh*, *Trh-Nfib*, *Trh-Omp*, *Trh-Tac1*, and *Trh-Ucn3* (Figure 1D). Notably, while the *Brs3-Adarb2* cluster was not annotated with a neuropeptide, it actually did express *Trh* (Figure S1C). This expression was present at relatively low levels compared with the other *Trh*$^+$ clusters and was found in a sequencing method-dependent manner (Figure S1C). As such, the *Brs3-Adarb2* population was included in further analyses pertaining to *Trh*$^+$ populations.

We then interrogated the expression of neuropeptidergic receptors in the various populations, to identify possible autocrine and paracrine signaling in the PVN (Figure 1E). Most populations expressed neuropeptidergic receptors that may facilitate local signaling, and some populations expressed receptors for their own neuropeptides.

2.2 | Neuroendocrine markers are enriched in distinct neuropeptide subpopulations

We next set out to identify which clusters may be linked to neuroendocrine function. In each neuropeptidergic type (Figure 2A), genes previously identified to be expressed in neuroendocrine cells were analyzed for presence in subpopulations. Furthermore, we compared similarities between subpopulations, revealing that not all neurons within a neuropeptide class were transcriptomically most similar to each other (Figure 2B). For instance, the *Oxt-Foxp1* neurons were more similar to the *Avp-Tac1* and *Avp-Th* neurons than the *Oxt-Adarb2*. In turn, the *Oxt-Adarb2* neurons were most similar to other *Adarb2*$^+$ neurons (Figure 2B).

To functionally classify the *Oxt*$^+$ neurons, we used the neuroendocrine *Oxt*$^+$ markers as described by Lewis et al.[5] In their study, a large overlap between magnocellular electrophysiology and neuroendocrine projection *Oxt*$^+$ neurons was found, and this magnocellular neuroendocrine population was reported to be enriched in *Calb1*, *Kcnmb4*, and *Foxp1*. Notably, a closer inspection of their single-cell data reveals that their magnocellular neuroendocrine cluster contains both *Avp*$^+$ and *Oxt*$^+$ neurons (Figure S3). Thus, these markers for the magnocellular neuroendocrine population are relevant to not only *Oxt*$^+$ neurons but also *Avp*$^+$ neurons.

In our data, these magnocellular neuroendocrine markers were found to be enriched in the *Oxt-Foxp1* cells relative to the *Oxt-Adarb2* cells, suggesting the former to be the neuroendocrine population (Figure 2C). Both *Avp-Tac1* and *Avp-Th* clusters were found to be strongly correlated with the magnocellular neuroendocrine *Oxt*$^+$ neurons (Figure 2B), whereas the *Avp-Adarb2* cluster was not. Furthermore, the *Avp-Tac1* and *Avp-Th* populations were enriched in the magnocellular neuroendocrine markers relative to *Avp-Adarb2* (Figure 2C). Between *Avp-Tac1* and *Avp-Th*, the *Avp-Th* population was slightly more enriched in these markers, but the relative differences were smaller than the difference in the *Avp-Adarb2* population or between *Oxt*$^+$ subpopulations.

Both the high degree of similarity between the *Avp-Tac1* and *Avp-Th* populations, and the expression of neuroendocrine markers in both populations imply *Avp-Tac1*, and *Avp-Th* may be magnocellular neuroendocrine *Avp*$^+$ neurons. It is currently not known if the differences between *Avp-Tac1* and *Avp-Th* neurons are functionally relevant, as the distinction has not been described before. It should be noted that, although positive for *Th*, the *Avp-Th* neurons do not

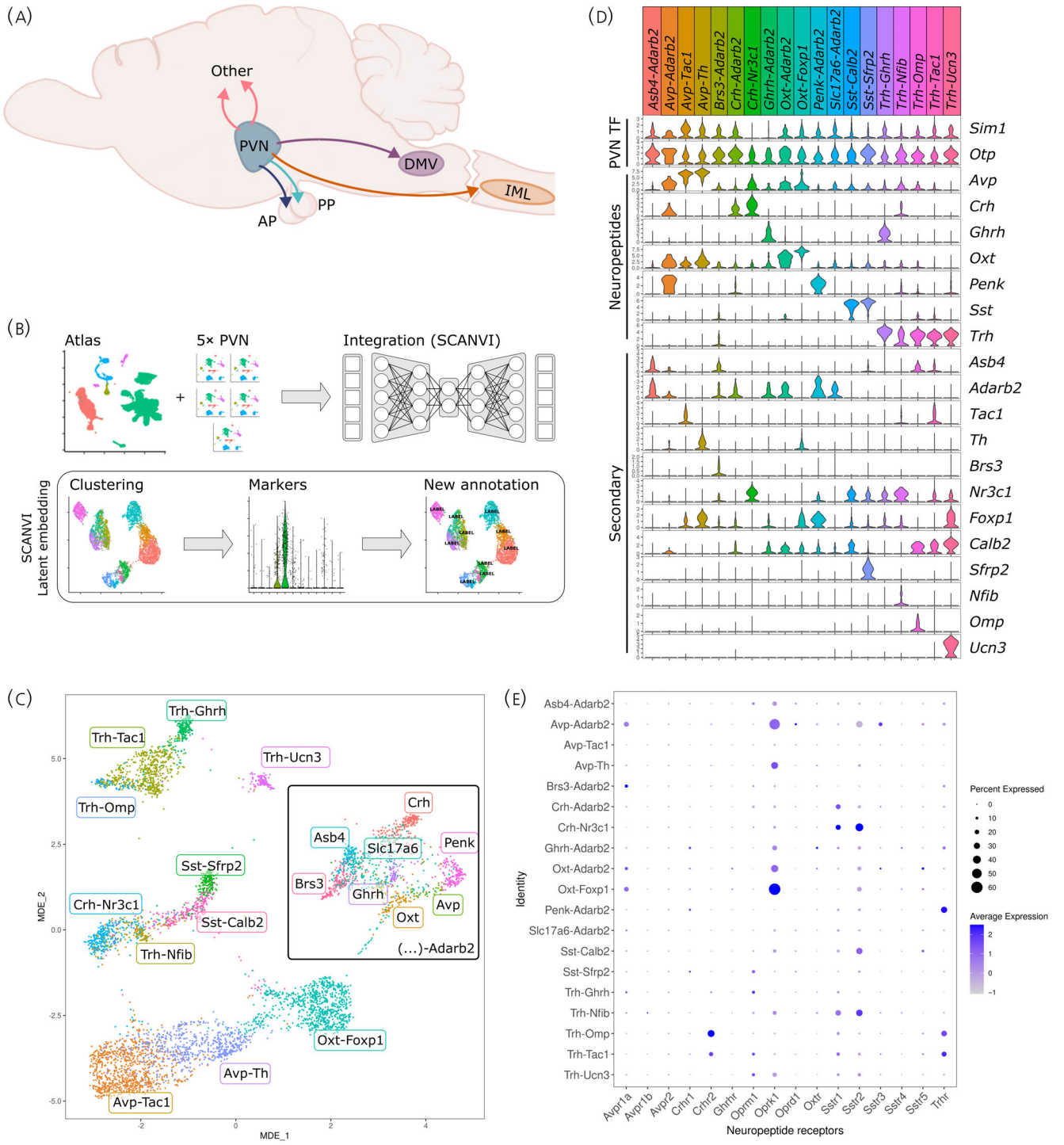

FIGURE 1 Neuropeptidergic paraventricular nucleus (PVN) neurons consist of multiple subpopulations. (A) Schematic showing the various projections from the PVN. Arrows point to the dorsal motor nucleus of the vagus (DMV), intermediolateral nucleus (IML), anterior pituitary (AP), and posterior pituitary (PP). Other central projections are denoted with the upward pink arrows. (B) Schematic of the methods used for this section. Five PVN datasets were integrated with the hypothalamus atlas (HypoMap) using scANVI. The integrated low-dimensional embedding was used for clustering and visualization. Clusters were annotated based on differential gene expression. (C) Minimally distorting embedding (MDE) representation of the datasets, with the cluster annotation based on neuropeptide markers and secondary gene markers. (D) Violin plots of the expression of PVN-specific transcription factors (TFs), neuropeptides, and secondary cluster markers. (E) Neuropeptidergic receptors in the various populations of the PVN. Dot size represents the percentage of cells expressing a gene, and dot color represents the average expression level.

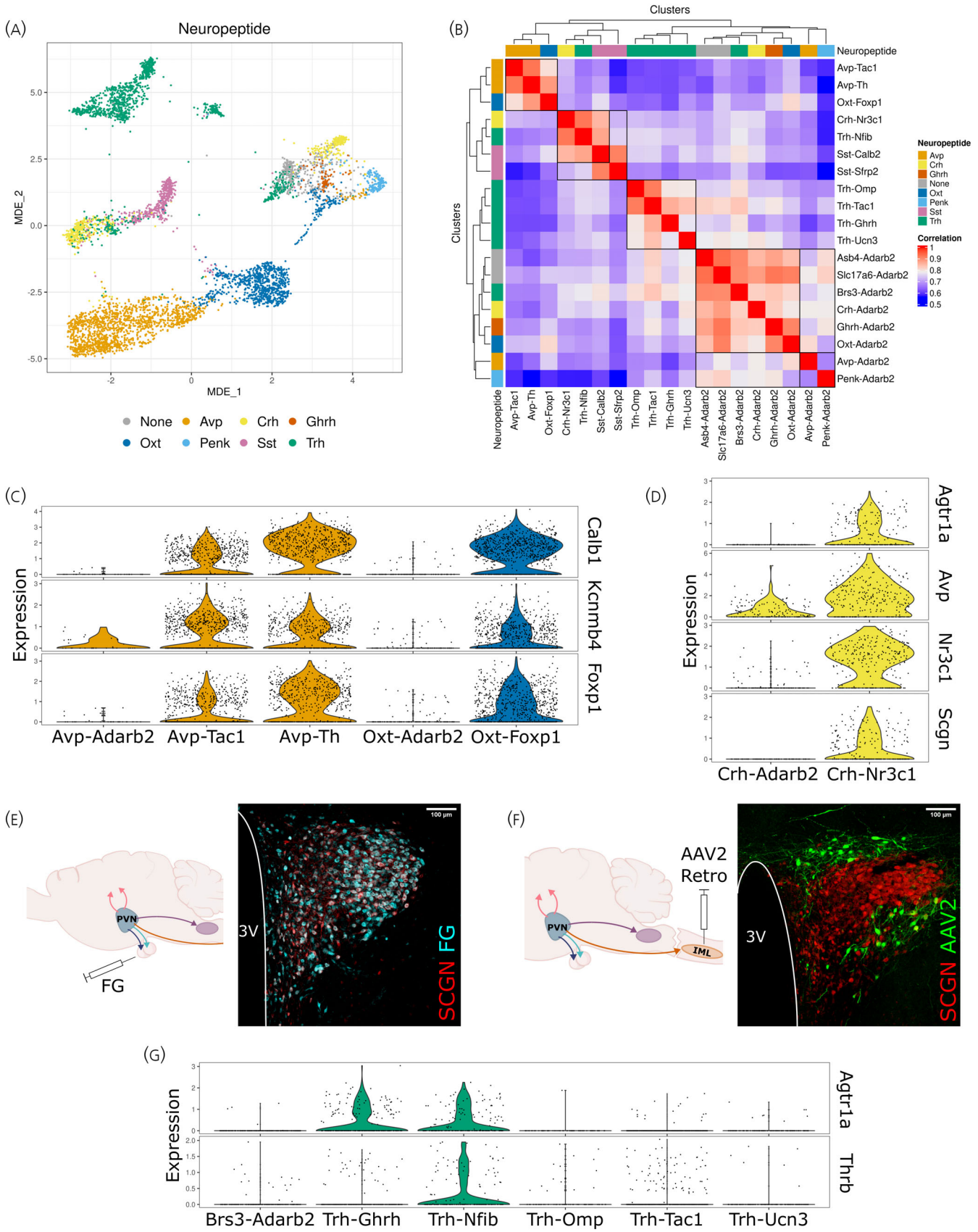

FIGURE 2 Legend on next page.

express *Ddc* (Figure S4A). Thus, these neurons cannot perform the final dopamine biosynthesis conversion, and therefore are not dopaminergic.

For the *Crh*$^+$ neurons, multiple markers for neuroendocrine function have been described. First and foremost, the glucocorticoid receptor (*Nr3c1*; GR) is an essential mediator of regulatory feedback in *Crh*$^+$ neurons of the HPA axis.[21] Another key component of these neurons is *Avp*, which strongly potentiates CRH-driven adrenocorticotropic hormone (ACTH) release from the anterior pituitary.[22] Further, *Scgn* has been proposed as a marker of neuroendocrine *Crh*$^+$ cells, as *Scgn* silencing abolishes stress-driven ACTH release.[23] Finally, *Agtr1a* has been found to be expressed in neuroendocrine *Crh*$^+$ and *Trh*$^+$ neurons.[24] All these markers were enriched in the *Crh-Nr3c1* population, suggesting these neurons to be the neuroendocrine *Crh*$^+$ population (Figure 2D). To validate this finding, we performed an immunofluorescence staining of SCGN in the rat PVN, combined with retrograde tracing of neuroendocrine and preautonomic neurons. Expression of SCGN was found to be highly colocalized with FluoroGold (FG)-labeled neuroendocrine neurons (Figures 2E and S4B). In contrast, no colocalization was found in SCGN with retrograde labeling of IML-projecting neurons (Figures 2F and S4B).

Like in *Crh*$^+$ neurons, neuroendocrine *Trh*$^+$ neurons are reported to express *Agtr1a*.[24] Additionally, literature indicates that the thyroid hormone receptor beta is critical to the T_3-mediated negative feedback on *Trh* expression.[25] Besides these two, other markers for neuroendocrine *Trh*$^+$ cells have not been described in the literature. While several *Trh*$^+$ populations expressed only one of these markers, only the *Trh-Nfib* neurons were enriched for both (Figure 2G), suggesting those to be the neuroendocrine population.

Finally, no markers specific for neuroendocrine *Sst*$^+$ subpopulations have been described in the literature. The identified clusters *Sst-Calb2* and *Sst-Sfrp2* do seem distinct in their expression of various genes. In *Sst-Sfrp2* neurons, *Sfrp2*, *Ar*, *Npy1r*, and *Mc4r* were enriched, whereas in the *Sst-Calb2* neurons, *Calb1*, *Calb2*, *Kcnip4*, and *Gpr101* were enriched (Figure S4C).

2.3 | Preautonomic neurons are embedded in the *Adarb2*$^+$ clusters

To identify preautonomic neurons in our data, we integrated a recent single-cell dataset that utilized retrograde tracing from the IML.[26] From this dataset, all neurons identified by the authors to be from the PVN were integrated into our PVN atlas. After integration, the traced neurons were embedded within the populations using *Adarb2* as secondary marker, here referred to as the *Adarb2*$^+$ populations (Figure 3A). Similar to the *Adarb2*$^+$ neurons, the traced neurons were high in their expression of *Adarb2*, *Reln*, *Snca*, and *Ntng1* (Figures 3B and S5A). Further similarity was found in the expression of *Cacna1g* (Figure S5B), a T-type calcium channel gene reported to mediate low-threshold spiking in preautonomic neurons.[27,28]

To further validate the association between *Adarb2*$^+$ neurons and preautonomic function, we did an immunofluorescence staining in the rat PVN for RELN, one of the *Adarb2*$^+$-enriched markers. We found strong colocalization of RELN with retrograde labeling of IML-projecting neurons (Figures 3C and S5B). In contrast, no colocalization was found in RELN with FG-labeled neuroendocrine neurons (Figures 3D and S5B).

We then analyzed *Adarb2*$^+$ subpopulations within the PVN atlas. Among the *Adarb2*$^+$ subpopulations, the traced neurons were embedded in particular within the *Avp-Adarb2*, *Oxt-Adarb2*, *Penk-Adarb2*, and *Crh-Adarb2* clusters (Figure 3E). The traced neurons expressed all these neuropeptides to some extent, though the expression of *Oxt* was markedly the most pronounced (Figure 3E).

Besides the IML, the preautonomic neurons of the PVN also project to the DMV. Although there are currently no retrograde tracing sequencing datasets available, a recent single-cell sequencing dataset of the general DMV[29] may still give insight into possibly relevant circuitry, through its neuropeptide receptor repertoire. In their study, Tao et al.[29] microdissected the DMV based on *Chat*-driven fluorescence and identified seven distinct DMV populations. We analyzed their dataset and found neuropeptidergic receptors that relate to PVN-expressed neuropeptides. The identified receptors were *Crhr1*, *Trhr*, *Sstr2*, *Sstr5*, *Oprm1*, *Oprd1*, and *Oxtr* (Figure S5C).

In summary, our results indicate that sympathetic preautonomic neurons include *Avp-Adarb2*, *Crh-Adarb2*, *Oxt-Adarb2*, and *Penk-Adarb2* neurons. Brainstem-projecting parasympathetic preautonomic neurons may be more diverse, with receptors for *Crh*, *Trh*, *Sst*, *Penk*, and *Oxt* present in the DMV.

2.4 | Centrally projecting populations are identified in the atlas

Finally, we set out to investigate the other central projections, upstream of the brainstem. While we assume that the *Trh-Omp*, *Trh-Ghrh*, and *Trh-Tac1* populations are centrally projecting, we unfortunately could not find any literature regarding the functional identities of these populations.

FIGURE 2 Expression of neuroendocrine markers in subpopulations of Avp$^+$, Oxt$^+$, Crh$^+$, and Trh$^+$ neurons. (A) Minimally distorting embedding (MDE) representation of the data, colored by neuropeptide class. Coloring identical to violin plot colors in panels (C,D,E). (B) Heatmap of correlations between clusters, calculated on pseudobulk expression values of highly variable genes. (C) Violin plots of the expression of neuroendocrine Avp$^+$ and Oxt$^+$ markers. (D) Violin plots of the expression of neuroendocrine Crh$^+$ markers. (E) Immunofluorescent staining of SCGN in the rat paraventricular nucleus (PVN), showing colocalization with FluoroGold (FG). (F) Immunofluorescent staining of SCGN in the rat PVN, showing no colocalization with retrograde tracing from the intermediolateral nucleus. (G) Violin plots of the expression of neuroendocrine Trh$^+$ markers.

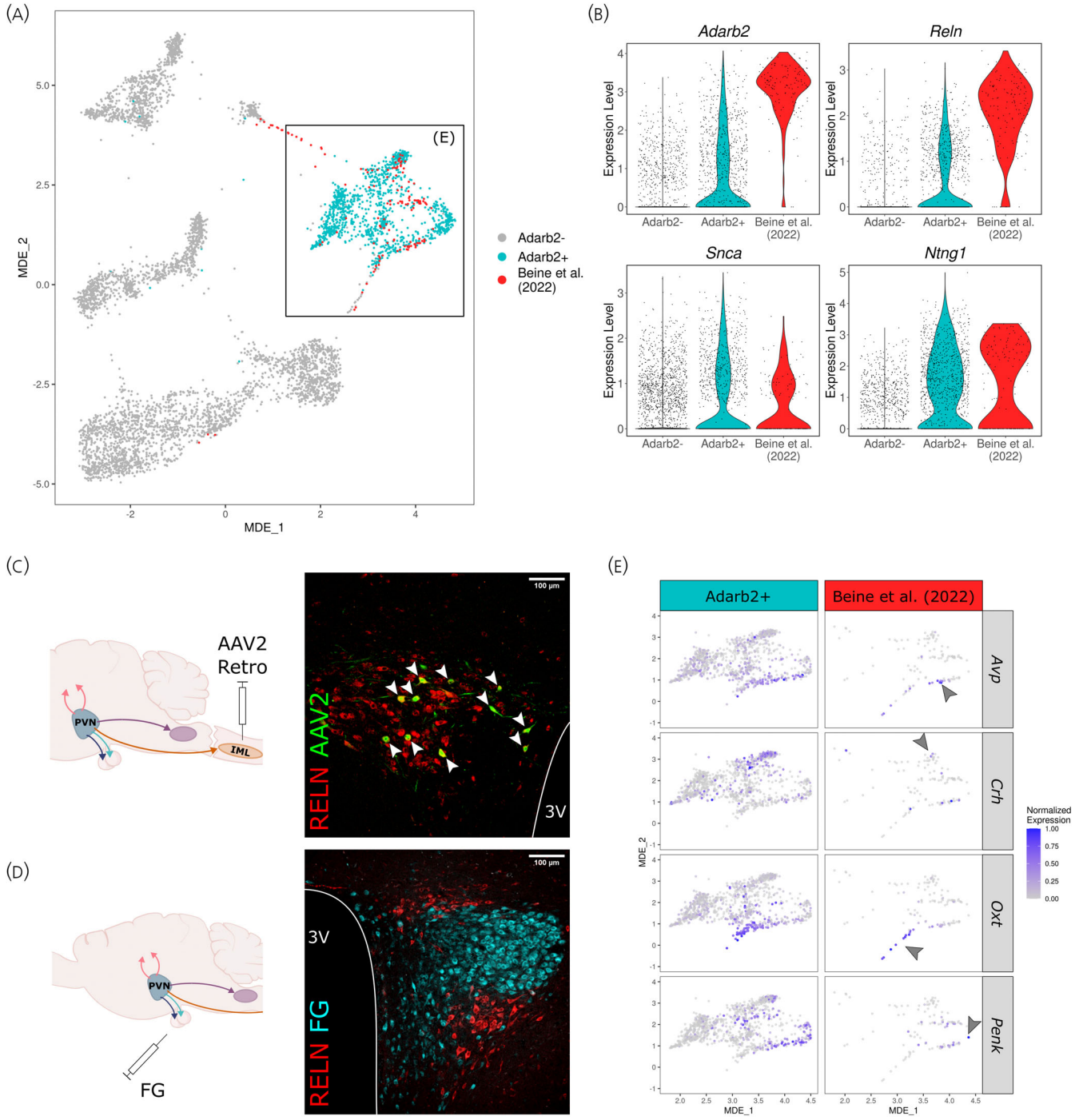

FIGURE 3 Preautonomic neurons cocluster with the Adarb2^{+} neurons. (A) Violin plots showing expression of Adarb2, Reln, Snca, and Ntng1 in the paraventricular nucleus (PVN) atlas and retrogradely traced PVN neuron from Beine et al.[26] (B) The minimally distorting embedding (MDE) representation, with cells from Beine et al.[26] highlighted in red. (C) Immunofluorescent staining of RELN in the rat PVN, showing colocalization with retrograde tracing from the intermediolateral nucleus. (D) Immunofluorescent staining of RELN in the rat PVN, showing no colocalization with FluoroGold (FG). (E) Zoomed-in MDE representation, showing the Adarb2^{+} clusters. Rows show cells from Beine et al.[26] and the rest of the dataset, and columns are split by expression of Avp, Crh, Oxt, and Penk.

The *Trh-Ucn3* population is synonymous with the perifornical population as described by Péterfi et al.,[30] Autry et al.,[31] and Horii-Hayashi et al.[32] Although generally described as perifornical, neurons of this *Ucn3*$^{+}$ population exist within the PVN boundaries[33] (Figure S6), hence its inclusion in our atlas. This population has been described as being involved in various behaviors, ranging from feeding,[30] to infant-directed aggression,[31] to risk assessment behavior.[32]

In addition to the *Trh-Ucn3* population, we investigated the *Mc4r*$^{+}$ population of the PVN, which has previously been described to

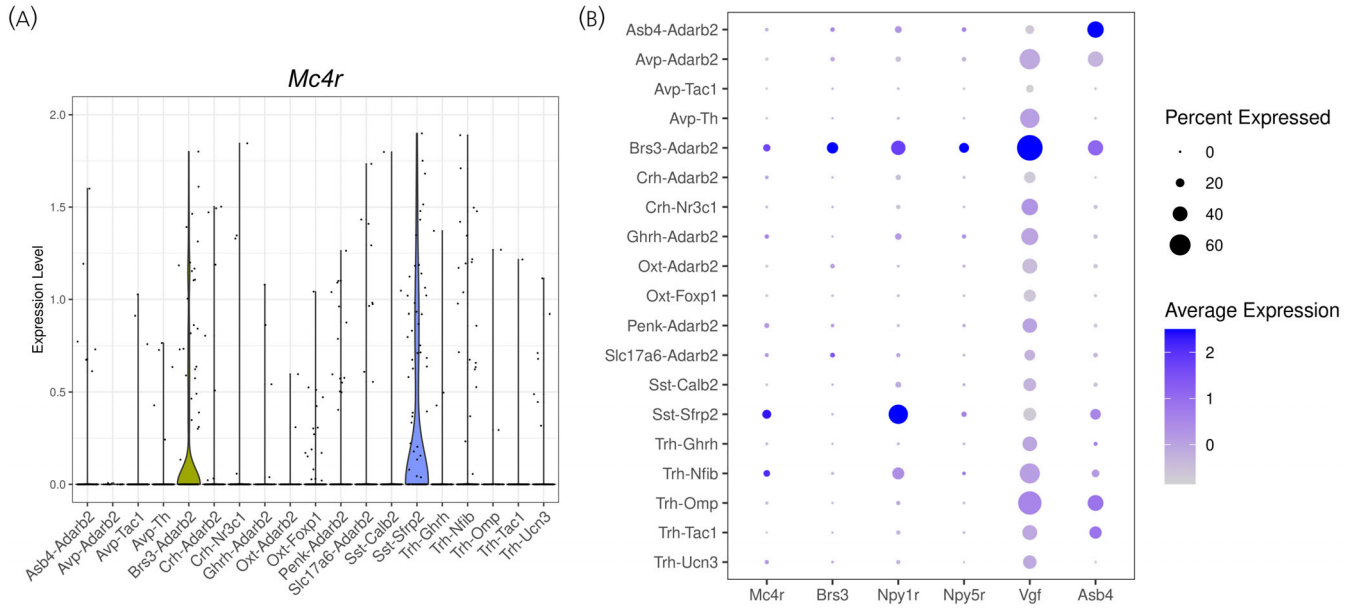

FIGURE 4 The Brs3-Adarb2 population expresses various feeding-related and energy expenditure-related genes, including Mc4r. (A) Violin plots showing the expression of Mc4r in the paraventricular nucleus (PVN) atlas. (B) Dot plot showing the expression of Mc4r, Brs3, Npy1r, Npy5r, Vgf, and Asb4 in the PVN atlas. Dot size represents the percentage of cells expressing a gene, and dot color represents the average expression level.

be involved in feeding behavior.[34,35] Expression of *Mc4r* is found in three populations, *Sst-Sfrp2* and *Brs3-Adarb2*, and to lesser extent *Trh-Nfib* (Figure 4A,B). In literature, the expression of *Mc4r* has been described in neuroendocrine *Trh*$^+$ and *Sst*$^+$ neurons.[36,37] Thus, the remaining undescribed *Brs3-Adarb2* population is left as an interesting candidate for the feeding-related *Mc4r*$^+$ population. Besides *Mc4r*, the *Brs3-Adarb2* population expresses *Brs3*, *Npy1r*, *Npy5r*, *Vgf*, and *Asb4* (Figure 4B). These genes have been associated with feeding behavior, suggesting the *Brs3-Adarb2* population to be involved in the control of feeding behavior.[35,38–42]

Interestingly, *Mc4r*, *Brs3*, *Npy1r*, and *Vgf* have also been associated with regulating energy expenditure through the sympathetic nervous system,[35,42,43] suggesting the *Brs3-Adarb2* population to also be involved in sympathetic outflow. This indicates that at least part of the preautonomic neurons may also project centrally, which further highlights the difficulty in comprehensively classifying the central projections of the PVN. Nevertheless, we were able to identify a putative population involved in feeding behavior and energy expenditure, while harmonizing existing literature on the various effector genes expressed within this population.

3 | DISCUSSION

In this study, we integrated single-cell PVN datasets into a general hypothalamic atlas and subsequently selected PVN-specific neurons from the integrated dataset. We characterized the resulting dataset, revealing multiple transcriptomic subpopulations for neuropeptidergic neurons. For the *Avp*$^+$, *Oxt*$^+$, *Crh*$^+$, and *Trh*$^+$ neurons, we identified distinct subpopulations that were enriched for neuroendocrine marker genes. We describe how spinally projecting preautonomic neurons cluster entirely with various *Adarb2*$^+$ neurons, and we identify putative neuropeptidergic types of brainstem-projecting preautonomic neurons. Finally, based on markers described in literature, we identify two putative populations involved in the central projections from the PVN.

Since we used a microdissected high-depth sequencing dataset as benchmark,[16] our final dataset is unlikely to contain any non-PVN neuron populations. Rare cell types for the PVN that are much more prominent in adjacent brain regions were excluded based on in situ hybridization data. Nonetheless, this approach also has its limitations, as the sample size of the benchmark dataset was relatively small. Rare transcriptomic populations, or populations restricted to undersampled PVN subregions, are less likely to be uncovered through this method.

Another limitation of our study is linked to the use of the retrogradely traced single-cell data from Beine et al.[26] Their study injected the retrograde tracer into the L1 spinal cord, while the IML spans from T2 through L2 in mice.[44] Thus, the traced population is likely only a limited representation of the spinally projecting preautonomic neurons, as the axon terminal location could be a source of transcriptomic variation in preautonomic neurons.

Despite the limitations, we were able to identify multiple subpopulations for all neuropeptidergic neuron populations previously shown to reside in the PVN. For *Avp*$^+$ neurons, we identified three distinct subpopulations that have not been described before: *Avp-Adarb2*, *Avp-Tac1*, and *Avp-Th*. While the presence of *Th* in *Avp*$^+$ neurons is not novel,[45] the presence of *Th* as marker for a distinct subpopulation of *Avp*$^+$ neurons has not been described before. The *Avp-Tac1* and *Avp-Th* subpopulations were highly correlated with the magnocellular

neuroendocrine *Oxt*$^+$ neurons, and both were high in expression of the neuroendocrine markers as described by Lewis et al.[5] These results indicate that these *Avp*$^+$ populations may be magnocellular neuroendocrine neurons. On the other hand, the *Avp-Adarb2* population was similar to the retrograde traced neuron, indicating a function as preautonomic neurons.

The identified *Oxt*$^+$ neuron subpopulations were transcriptomically the same as identified by Lewis et al.[5]—with the side note that the magnocellular population in their dataset was composed of both *Avp*$^+$ and *Oxt*$^+$ neuroendocrine neurons. We identify the *Oxt-Foxp1* neurons to be the magnocellular neuroendocrine *Oxt*$^+$ population and identify the parvocellular *Oxt-Adarb2* neurons to be preautonomic, based on the transcriptomic overlap with retrogradely traced neurons. However, it is important to note that *Oxt-Adarb2* neurons are not only functionally preautonomic but also centrally projecting. For instance, these neurons project to nucleus accumbens and nucleus of the solitary tract.[5,9]

For the *Crh*$^+$ neurons, two subpopulations were identified: *Crh-Nr3c1* and *Crh-Adarb2*. These *Crh*$^+$ subpopulations are synonymous to the populations, as discussed by Romanov and Harkany[46]: *Crh-Scgn* and *Crh-Fam150b*, respectively. While these markers would have worked for our *Crh*$^+$ populations as well, clusters were annotated with different markers more fitting for the context of our dataset. We found that the *Crh-Nr3c1* neurons were enriched for multiple neuroendocrine markers genes, while the *Crh-Adarb2* neurons were transcriptomically similar to a subset of spinally projecting preautonomic neurons. In contrast, Romanov and Harkany[46] posit that both subpopulations are neuroendocrine and that other markers—like *Npy1r*—define subsets of these populations that are preautonomic instead of neuroendocrine. We do not find any evidence for this theory. First, neuroendocrine markers like *Agtr1a*, *Nr3c1*, and *Scgn* are lacking entirely in the *Crh-Adarb2* neurons, while *Avp* was also relatively low in expression in these cells. Second, no retrogradely traced preautonomic neurons were found coclustering with the *Crh-Nr3c1* neurons. Finally, our immunofluorescence validations do not support a preautonomic function of the *Scgn*-expressing *Crh-Nr3c1* subpopulation nor a neuroendocrine function of *Reln*-expressing Crh-*Adarb2* neurons. Together, this suggests that these two *Crh*$^+$ subpopulations are functionally distinct.

Multiple subpopulations of *Trh*$^+$ neurons were also identified in our analysis, but the functional interpretation [for these Trh subpopulations] was more difficult than [the functional interpretation] for other [non-Trh] populations. We observed an enrichment of two neuroendocrine markers in *Trh-Nfib* neurons. Aside from neuroendocrine function, only the *Trh-Ucn3* population could be functionally resolved. We identify this population to be synonymous with the perifornical *Ucn3*$^+$ population. Although generally described as perifornical, neurons from this population reside in the PVN as well. The population has been implicated in various behaviors, including feeding, infant-directed aggression, and risk assessment behavior.[30–32]

The identified *Sst*$^+$ subpopulations could not be linked to a functional identity due to lacking literature on functional *Sst*$^+$ subpopulations. Despite this, two of the identified differential genes do stand out. First, the *Ar* has been described in literature to define a subgroup of *Sst*$^+$ neurons that is present in both sexes, but in larger numbers in males.[47] This population is postulated to be relevant for sexually dimorphic action of SST on the HPS axis. The other notable gene is *Gpr101*, which has been reported as the causative gene to X-linked acrogigantism—a disorder involving the growth hormone axis.[48] Since both populations can be linked to the HPS axis, through either *Ar* or *Gpr101*, we hypothesize that both subpopulations are neuroendocrine in nature, with the two populations acting as separate substrates for HPS axis inhibition.

Furthermore, we analyzed the neuropeptide receptor repertoire of the DMV. Receptors for CRH, OXT, PENK, and SST were present, as well as the receptor for TRH to a lesser extent. This receptor expression profile is consistent with literature on PVN-DMV neurons, which reports the expression of AVP, OXT, PENK, SST, and CRH in preparasympathetic neurons.[8,49] The presence of TRH receptor might indicate relevance for this neuropeptide in PVN-DMV circuitry as well, though TRH projections could also originate from brain regions other than the PVN. As the DMV-projecting AVP and OXT neurons were reportedly parvocellular, we can infer that the *Avp-Adarb2* and *Oxt-Adarb2* populations are the most likely candidates for the vasopressinergic and oxytocinergic PVN-DMV connections. This would implicate these populations in both presympathetic and preparasympathetic functions, with currently no known differentiating factor to define these functional subpopulations. In summary, our findings reinforce and expand on current literature on PVN-DMV circuitry and introduce novel avenues to elucidate neuropeptidergic subpopulations involved in this circuit.

Finally, we characterized some central projections of the PVN. We identified a likely candidate for the feeding-related *Mc4r*$^+$ population, *Brs3-Adarb2*. Genes expressed in this population have been associated with feeding behavior, as well as energy expenditure through sympathetic outflow.[35,38–42] Like the *Oxt-Adarb2* population, the *Brs3-Adarb2* population seems to be involved in both preautonomic and central functions. It is unclear whether the dual-function populations are homogenous, in which these functions are inseparably linked, or if discrete subpopulations may be responsible for these different functions. Further research and data are needed to increase the resolution of these populations, and thereby resolve this question.

In conclusion, our study presents a detailed overview of the neuronal transcriptomic subpopulations in the PVN and attempts to resolve functional identities for the identified populations (Figure 5). The study pinpoints interesting markers of neuropeptidergic subpopulations that may be used for research into functionalities that are specifically associated with these subpopulations.

4 | METHODS

4.1 | scRNA-seq data collection and preprocessing

PVN scRNA-seq datasets were acquired from the relevant Gene Expression Omnibus (GEO) repositories (Table 1). The hypothalamic

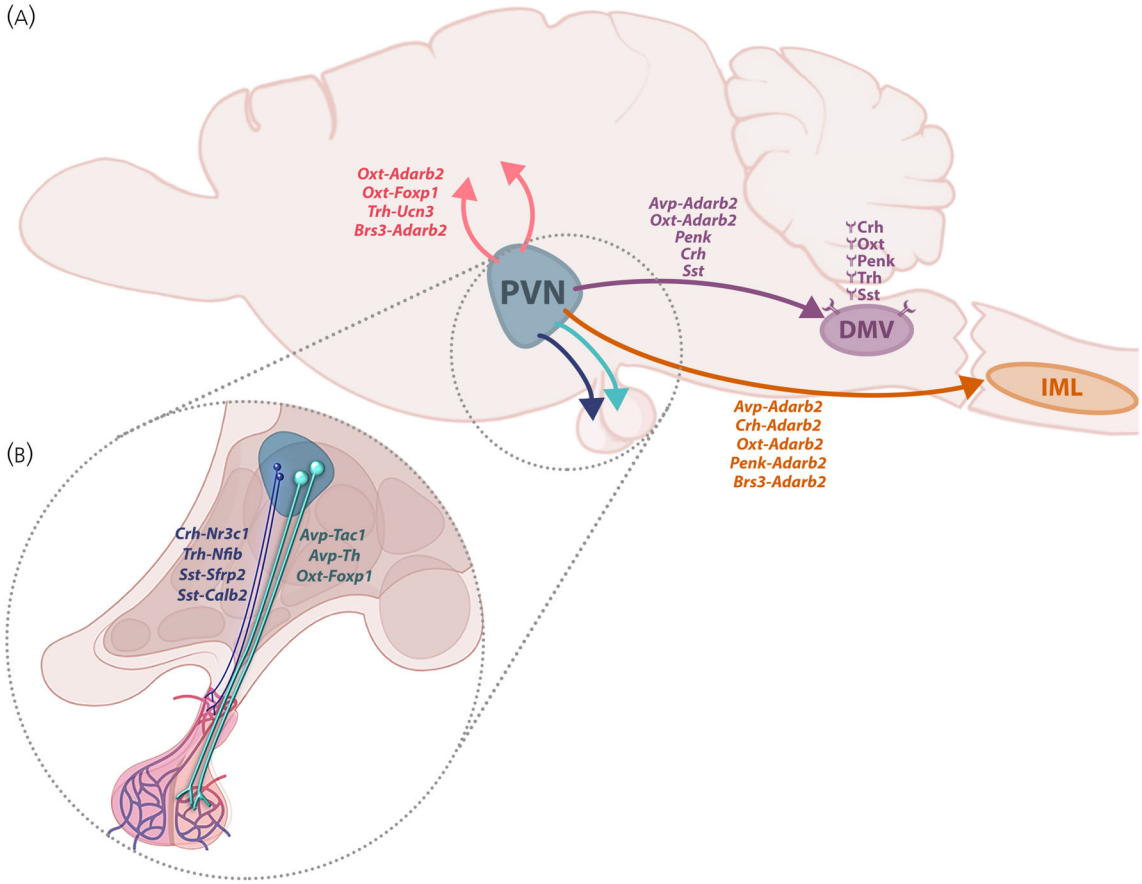

FIGURE 5 Summarized findings from our PVN atlas. (A) Overview of projections from the paraventricular nucleus (PVN) to the intermediolateral nucleus (IML), dorsal motor nucleus of the vagus (DMV), and other central projections with relevant cell populations indicated. Neuropeptides and neuropeptide receptors are shown, where exact clusters could not be identified. (B) Overview of projections from the PVN to the pituitary, with relevant cell populations shown.

TABLE 1 Datasets used in this article.

Reference	GEO/CxG	Technology	Cell type/region	Cells included	Counts/cell
Beine et al.[26]	GSE212409	10× v3	Includes PVN	142	2546
Lewis et al.[5]	GSE147092	SMART-Seq2	*Oxt*$^{+}$	134	1,146,706
Lopez et al.[13]	GSE161751	10× v2	PVN	6399	8860
Short et al.[14]	GSE174085	SMART-Seq2	*Crh*$^{+}$	519	1,494,713
Steuernagel et al.[1]	HypoMap	10× v1, v2, v3; Drop-Seq	Hypothalamus	384,925	4812
Son et al.[15]	GSE166616	Drop-seq	*Sim1*$^{+}$	2440	7679
Tao et al.[29]	GSE172411	Smart-Seq2	DMV	282	1,539,569
Xu et al.[16]	GSE148568	SMART-SCRB	PVN	706	177,416

Abbreviation: CxG, CELLxGENE.

atlas data (HypoMap) were acquired from CELLxGENE (Table 1). Each dataset was preprocessed separately to filter low-quality cells based on transcript count, gene count, and percentage of mitochondrial gene expression (Table S1). Datasets using Ensembl IDs were converted to MGI symbols. Furthermore, dataset metadata was standardized to include assay, disease, organism, sex, SRA_ID, Sample_ID, and Dataset, using the HypoMap atlas metadata as template. Within the atlas, cells were annotated at various levels of granularity, ranging from C7_named to C465_named. The number in these annotation levels denotes the number of clusters at that annotation level. Nonatlas datasets were annotated at the C7_named level by comparison of cluster marker genes with the respective expression patterns in the atlas, assigning clusters in the nonatlas dataset based on these comparisons. Finally, the datasets were merged on the raw counts and

metadata. For further analysis, we selected neuronal cells only, based on the C7_named annotation key. Additionally, the first principal component of the immediate early genes (IEGs) *Fos*, *Fosb*, *Jun*, *Junb*, *Egr1*, *Egr2*, *Npas4*, *Nr4a1*, *Nr4a2*, and *Nr4a3* was calculated on normalized gene expression, to regress out the effect of IEGs during integration.

4.2 | scRNA-seq data integration

The highly variable genes of the merged dataset were selected using the function highly_variable_genes from scanpy[50] with parameters n_top_genes = 2500, flavor = "seurat," subset = True, and batch_key = "Dataset." Using scVI,[18] the dataset was then integrated on Sample_ID with assay, suspension_type and sex as categorical covariates, and with immediate_early and pctMito_RNA as continuous covariates. The model used parameters n_layers = 3, n_latent = 20, dropout_rate = 0.01, dispersion = "gene-cell," and gene_likelihood = "zinb." The model was trained for 400 epochs, with n_epochs_kl_warmup = 400, lr = 0.01, lr_min = 0.0001, reduce_lr_on_plateau = True, lr_patience = 8, lr_factor ≈ 0.56, and lr_scheduler_metric = "elbo_validation." The resulting trained scVI model was passed to scANVI.[17] The scANVI model was then trained for 250 epochs, using C66_named as label key. The scANVI model was trained using the same parameters as scVI, except for classification_ratio = 200 and n_epochs_kl_warmup = 100. Both scVI and scANVI models were trained with early stopping, using early_stopping = True, early_stopping_patience = 25, early_stopping_monitor = "elbo_validation" as parameters.

To isolate PVN-specific cells from the integrated dataset, the cells from Xu et al.[16] were used as benchmark. In that study, PVN boundaries were identified based on fluorescent agouti-related peptide (AgRP) axon tracts, and PVN neurons were microdissected and sequenced using a plate-based sequencing method (SMART-SCRB). The resulting dataset was thus deemed the most accurate representation of the PVN because of the combination of high sequencing depth and precise cell isolation method used. The other PVN datasets were either selective for a single neuropeptide neuron type, or not fully specific for the PVN, due to contamination with neurons from bordering regions.

As such, a subset was taken of predicted C66_named clusters that contained five or more cells originating from Xu et al.[16] This subset was clustered using the Leiden algorithm[51] with n_neighbors = 30 and resolution = 1. A subset was taken of the resulting clusters, again retaining only clusters with at least five cells from Xu et al.[16] These subsetting steps retained 98.58% and 97.56% of the cells from Xu et al.,[16] respectively. The resulting subset was then reintegrated using the same steps and parameters as before, except for the highly variable gene selection with n_top_genes = 1000.

The scANVI latent embedding was used to cluster the data with the Leiden algorithm[51] with n_neighbors = 30 and resolution = 1. Each of the resultant 20 clusters was analyzed for the presence of Xu et al.[16] neurons. Only clusters with the presence of minimally five of these neurons were annotated. An exception was made for *Trh-Ucn3*, as Allen Brain Atlas in situ hybridization data showed *Ucn3* expression in the PVN (Figure S6). For annotation, these clusters were tested for potential subclusters using the FindSubClusters function, and subclusters containing no cells from Xu et al.[16] were excluded. The resultant clusters and subclusters were tested for enriched genes using the FindMarkers functions and were annotated accordingly. Finally, a subset was taken with all annotated clusters, containing only the annotated populations described in the Results section.

To analyze the retrogradely traced neurons from Beine et al.,[26] the PVN neurons within that dataset were selected based on *Sim1* expression. The selected neurons were integrated into the PVN atlas, using the same steps and parameters for scANVI integration as described before. Altered parameters were n_top_genes = 1000 and early_stopping = False. The latent representation of this final integration was used for visualization of the data, using the preserve_neighbors function from the minimally distorting embedding (MDE) framework.[52] Parameters used for MDE visualization were attractive_penalty = Huber, repulsive_penalty = Log, n_neighbors = 30, and device = "cuda."

Finally, for the analysis of the neuropeptide receptors in the DMV, preprocessing and clustering steps as described by Tao et al.[29] were replicated.

4.3 | Animals

Adult male Wistar rats (Charles River, Germany) weighing 200–250 g were group-housed in a 12/12-h light/dark cycle with ad libitum access to food and water. All animal experiments were carried out in accordance with the guidelines of the Animal Ethics Committee of the Royal Dutch Academy of Arts and Sciences (KNAW, Amsterdam, The Netherlands) and approved by the Netherlands Institute for Neuroscience (NIN, Amsterdam, The Netherlands).

4.4 | Production of virus

The AAV2-retro-CAG-nls-GFP virus was prepared following the protocol as outlined by Verhaagen et al.[53] Briefly, HEK293T cells were cultured in 15 cm dishes with DMEM containing 10% fetal calf serum and penicillin/streptomycin. The next day, the cells were cotransfected with AAV2-retro serotype helper plasmid,[54] helper plasmid pAdδ F6, and pAAV-CAG-nls-GFP[55] using PEI (polyethylenimine 25 kDa, linear). After 72 h of transfection, the cells were harvested, lysed, and centrifuged. Viral particles were purified from the supernatant using iodixanol density gradient centrifugation with an Amicon Ultra-15 centrifugal filter. The final viral titers were determined by quantitative polymerase chain reaction for the WPRE gene in the viral genome (vg) using the following primers: 5′-GTGTTGCCACCTGGATT-3′ and 5′-CGAAGGGACGTAGCAGAA-3′. The titer of the viral batch used was 4E+12 vg/mL.

4.5 | Surgical procedures

Rats were anesthetized by an intramuscular injection of Medetomidine (0.26 mg/kg) and ketamine (64 mg/kg) mix. For the retrograde tracing of the preautonomic motor neurons in the PVN, the spinal cord was carefully exposed via a small laminectomy. Two to three microliters of AAV2-retro-CAG-nls-GFP virus was delivered to the IML column of the spinal cord at T5–T8 using a Nanoject III, and coordinates 0.05 mm lateral and 0.1 mm ventral from the surface of the spinal cord. The glass capillary needle was left in place for 2 min after the injection to minimize leakage of the virus. Animals were sacrificed for further analysis after 4 weeks. To target the neuroendocrine neurons in the PVN, an intraperitoneal injection of 2% (w/v) FG (Santa Cruz Biotechnology) was carried out with a survival time of 1 week. Because of the leaky blood–brain barrier at the median eminence and posterior pituitary, FG is taken up by the axonal terminals of PVN neuroendocrine neurons.

4.6 | Tissue preparation

The animals were anesthetized with an overdose of Pentobarbital and then perfused transcardially with 150 mL of 0.9% saline, followed by 200 mL of cold 4% paraformaldehyde in a phosphate-buffered (0.1 M, pH 7.4) solution. The brains were collected and left in 4% paraformaldehyde for postfixation overnight and then transferred to 30% sucrose until the tissue sank to the bottom of the container. The tissue was embedded in Tissue-Tek O.C.T. Compound and sectioned at 35 m using a Leica Biosystems Cryostat.

4.7 | Immunofluorescence staining

PVN sections with neuro-endocrine or preautonomic labeled neurons were incubated with guinea pig anti-SCGN (Synaptic systems no. 436004) or mouse anti-RELN (Sigma-Aldrich no. MAB5364) at 1:500 dilution with 10% normal donkey serum (Abcam) overnight at 4°C. Alexa Fluor 594 donkey antimouse (ThermoFisher no. R37115) and Alexa Fluor 594 donkey antiguinea pig (Jackson Immunoresearch no. 706585148) secondary antibodies at 1:400 dilution for 60–90 min at room temperature were used to detect RELN and SCGN. Antibodies were diluted in super mix solution containing 0.25% (w/v) gelatin and 0.5% (v/v) Triton X-100 in tris-buffered saline (TBS; pH 7.6). Sections were rinsed three times for 10 min with TBS between incubations to remove residual substances. The sections were fixed onto gelatin-coated slides and coverslipped with VectaShield mounting medium. Images were acquired using a Leica SP8 confocal microscope.

4.8 | Statistics

Single-cell transcriptomics pipelines and statistical computations were performed using both Python 3.7.10 and R 4.1.2.[56] Packages used for the analysis were tidyverse 2.0.0, Seurat 4.3.0.1, ComplexHeatmap 2.15.4, scanpy 1.9.1, scvi-tools 0.16.3, and all respective dependencies.

AUTHOR CONTRIBUTIONS

J. B. Berkhout: Formal analysis; investigation; software; visualization; writing—original draft. **D. Poormoghadam:** Investigation; validation; visualization; writing—original draft. **C. Yi:** Conceptualization; funding acquisition; supervision. **A. Kalsbeek:** Conceptualization; funding acquisition; supervision; writing—review and editing. **O. C. Meijer:** Funding acquisition; supervision; writing—review and editing. **A. Mahfouz:** Funding acquisition; supervision; writing—review and editing.

ACKNOWLEDGEMENTS

We would like to thank Fred de Winter for providing the AAV2-retro-CAG-nls-GFP virus for us, and his continued support during the study.

FUNDING INFORMATION

This research was funded by ZonMw Open Competition (grant no. 09120012010051).

CONFLICT OF INTEREST STATEMENT

The authors declare no conflict of interest.

PEER REVIEW

The peer review history for this article is available at https://www.webofscience.com/api/gateway/wos/peer-review/10.1111/jne.13367.

DATA AVAILABILITY STATEMENT

Reproducible code for the generation of the dataset and figures is available at https://github.com/jberkh/2023_PVN_Atlas. The integrated PVN atlas can be found at Zenodo (https://doi.org/10.5281/zenodo.8160037) and will be published to CELLxGENE.

ORCID

J. B. Berkhout https://orcid.org/0000-0002-0776-6995
D. Poormoghadam https://orcid.org/0000-0003-1669-4775
C. Yi https://orcid.org/0000-0003-1184-4615
A. Kalsbeek https://orcid.org/0000-0001-9606-8453
O. C. Meijer https://orcid.org/0000-0002-8394-6859
A. Mahfouz https://orcid.org/0000-0001-8601-2149

REFERENCES

1. Steuernagel L, Lam BYH, Klemm P, et al. HypoMap—a unified single-cell gene expression atlas of the murine hypothalamus. *Nat Metab*. 2022;4(10):1402-1419. doi:10.1038/s42255-022-00657-y
2. Biag J, Huang Y, Gou L, et al. Cyto- and chemoarchitecture of the hypothalamic paraventricular nucleus in the C57BL/6J male mouse: a study of immunostaining and multiple fluorescent tract tracing. *J Comp Neurol*. 2012;520(1):6-33. doi:10.1002/cne.22698
3. Ferris CF, Melloni Jr RH, Koppel G, Perry KW, Fuller RW, Delville Y. Vasopressin/serotonin interactions in the anterior hypothalamus

control aggressive behavior in Golden hamsters. *J Neurosci*. 1997; 17(11):4331-4340. doi:10.1523/JNEUROSCI.17-11-04331.1997

4. van Leengoed E, Kerker E, Swanson HH. Inhibition of post-partum maternal behaviour in the rat by injecting an oxytocin antagonist into the cerebral ventricles. *J Endocrinol*. 1987;112(2):275-282. doi:10.1677/joe.0.1120275
5. Lewis EM, Stein-O'Brien GL, Patino AV, et al. Parallel social Information processing circuits are differentially impacted in autism. *Neuron*. 2020;108(4):659-675.e6. doi:10.1016/j.neuron.2020.10.002
6. Cechetto DF, Saper CB. Neurochemical organization of the hypothalamic projection to the spinal cord in the rat. *J Comp Neurol*. 1988; 272(4):579-604. doi:10.1002/cne.902720410
7. Hallbeck M, Larhammar D, Blomqvist A. Neuropeptide expression in rat paraventricular hypothalamic neurons that project to the spinal cord. *J Comp Neurol*. 2001;433(2):222-238. doi:10.1002/cne.1137
8. Sawchenko PE, Swanson LW. Immunohistochemical identification of neurons in the paraventricular nucleus of the hypothalamus that project to the medulla or to the spinal cord in the rat. *J Comp Neurol*. 1982;205(3):260-272. doi:10.1002/cne.902050306
9. Knobloch HS, Charlet A, Hoffmann LC, et al. Evoked axonal oxytocin release in the central amygdala attenuates fear response. *Neuron*. 2012;73(3):553-566. doi:10.1016/j.neuron.2011.11.030
10. Hung LW, Neuner S, Polepalli JS, et al. Gating of social reward by oxytocin in the ventral tegmental area. *Science*. 2017;357(6358): 1406-1411. doi:10.1126/science.aan4994
11. Grinevich V, Neumann ID. Brain oxytocin: how puzzle stones from animal studies translate into psychiatry. *Mol Psychiatry*. 2021;26(1): 265-279. doi:10.1038/s41380-020-0802-9
12. Rigney N, de Vries GJ, Petrulis A. Modulation of social behavior by distinct vasopressin sources. *Front Endocrinol*. 2023;14:1127792. doi: 10.3389/fendo.2023.1127792
13. Lopez JP, Brivio E, Santambrogio A, et al. Single-cell molecular profiling of all three components of the HPA Axis reveals adrenal ABCB1 as a regulator of stress adaptation. *Sci Adv*. 2021;7(5):eabe4497. doi: 10.1126/sciadv.abe4497
14. Short AK, Thai CW, Chen Y, et al. Single-cell transcriptional changes in hypothalamic corticotropin-releasing factor-expressing neurons after early-life adversity inform enduring alterations in vulnerabilities to stress. *Biol Psychiatry Glob Open Sci*. 2021;3:99-109. doi:10.1016/j.bpsgos.2021.12.006
15. Son JE, Dou Z, Wanggou S, et al. Ectopic expression of Irx3 and Irx5 in the paraventricular nucleus of the hypothalamus contributes to defects in Sim1 Haploinsufficiency. *Sci Adv*. 2021;7(44):eabh4503. doi:10.1126/SCIADV.ABH4503
16. Xu S, Yang H, Menon V, et al. Behavioral state coding by molecularly defined paraventricular hypothalamic cell type ensembles. *Science*. 2020;370(6514):eabb2494. doi:10.1126/science.abb2494
17. Xu C, Lopez R, Mehlman E, Regier J, Jordan MI, Yosef N. Probabilistic harmonization and annotation of single-cell Transcriptomics data with deep generative models. *Mol Syst Biol*. 2021;17(1):e9620. doi:10.15252/msb.20209620
18. Lopez R, Regier J, Cole MB, Jordan MI, Yosef N. Deep generative modeling for single-cell Transcriptomics. *Nat Methods*. 2018;15(12): 1053-1058. doi:10.1038/s41592-018-0229-2
19. McIntyre C, Li XF, Ivanova D, Wang J, O'Byrne KT. Hypothalamic PVN CRH neurons signal through PVN GABA neurons to suppress GnRH pulse generator frequency in female mice. *Endocrinology*. 2023; 164(6):bqad075. doi:10.1210/endocr/bqad075
20. Gainer H. Cell-type specific expression of oxytocin and vasopressin genes: an experimental odyssey. *J Neuroendocrinol*. 2012;24(4):528-538. doi:10.1111/j.1365-2826.2011.02236.x
21. Herman JP, McKlveen JM, Ghosal S, et al. Regulation of the hypothalamic-pituitary-adrenocortical stress response. *Compr Physiol*. 2016;6(2):603-621. doi:10.1002/cphy.c150015
22. Gillies GE, Linton EA, Lowry PJ. Corticotropin releasing activity of the new CRF is potentiated several times by vasopressin. *Nature*. 1982; 299(5881):355-357. doi:10.1038/299355a0
23. Romanov RA, Alpár A, Zhang M-D, et al. A Secretagogin locus of the mammalian hypothalamus controls stress hormone release. *EMBO J*. 2015;34(1):36-54. doi:10.15252/embj.201488977
24. de Kloet AD, Wang L, Pitra S, et al. A unique 'angiotensin-sensitive' neuronal population coordinates neuroendocrine, cardiovascular, and behavioral responses to stress. *J Neurosci*. 2017;37(13):3478-3490. doi:10.1523/JNEUROSCI.3674-16.2017
25. Nillni EA. Regulation of the hypothalamic thyrotropin releasing hormone (TRH) neuron by neuronal and peripheral inputs. *Front Neuroendocrinol*. 2010;31(2):134-156. doi:10.1016/j.yfrne.2010.01.001
26. Beine Z, Wang Z, Tsoulfas P, Blackmore MG. Single nuclei analyses reveal transcriptional profiles and marker genes for diverse Supraspinal populations. *J Neurosci*. 2022;42(47):8780-8794. doi:10.1523/JNEUROSCI.1197-22.2022
27. Feetham CH, O'Brien F, Barrett-Jolley R. Ion channels in the paraventricular hypothalamic nucleus (PVN); emerging diversity and functional roles. *Front Physiol*. 2018;9(July):760. doi:10.3389/fphys.2018.00760
28. Lee S, Han TH, Sonner PM, Stern JE, Ryu PD, Lee SY. Molecular characterization of T-type Ca2+ channels responsible for low threshold spikes in hypothalamic paraventricular nucleus neurons. *Neuroscience*. 2008;155(4):1195-1203. doi:10.1016/j.neuroscience.2008.06.055
29. Tao J, Campbell JN, Tsai LT, Chen W, Liberles SD, Lowell BB. Highly selective brain-to-gut communication via genetically defined Vagus neurons. *Neuron*. 2021;109(13):2106-2115.e4. doi:10.1016/j.neuron.2021.05.004
30. Péterfi Z, Farkas E, Nagyunyomi-Sényi K, et al. Role of TRH/UCN3 neurons of the Perifornical area/bed nucleus of Stria Terminalis region in the regulation of the Anorexigenic POMC neurons of the arcuate nucleus in male mice and rats. *Brain Struct Funct*. 2018; 223(3):1329-1341. doi:10.1007/s00429-017-1553-5
31. Autry AE, Wu Z, Kapoor V, et al. Urocortin-3 neurons in the mouse Perifornical area promote infant-directed neglect and aggression. *eLife*. 2021;10(August):e64680. doi:10.7554/eLife.64680
32. Horii-Hayashi N, Nomoto K, Endo N, Yamanaka A, Kikusui T, Nishi M. Hypothalamic Perifornical Urocortin-3 neurons modulate defensive responses to a potential threat stimulus. *iScience*. 2021;24(1):101908. doi:10.1016/j.isci.2020.101908
33. Wittmann G, Füzesi T, Liposits Z, Lechan RM, Fekete C. Distribution and axonal projections of neurons Co-expressing thyrotropin-releasing hormone and Urocortin 3 in the rat brain. *J Comp Neurol*. 2009;517(6):825-840. doi:10.1002/cne.22180
34. Li MM, Madara JC, Steger JS, et al. The paraventricular hypothalamus regulates satiety and prevents obesity via two genetically distinct circuits. *Neuron*. 2019;102(3):653-667.e6. doi:10.1016/j.neuron.2019.02.028
35. Singh U, Jiang J, Saito K, et al. Neuroanatomical organization and functional roles of PVN MC4R pathways in physiological and behavioral regulations. *Mol Metab*. 2022;55(January):101401. doi:10.1016/j.molmet.2021.101401
36. Decherf S, Seugnet I, Kouidhi S, Lopez-Juarez A, Clerget-Froidevaux M-S, Demeneix BA. Thyroid hormone exerts negative feedback on hypothalamic type 4 Melanocortin receptor expression. *Proc Natl Acad Sci U S A*. 2010;107(9):4471-4476. doi:10.1073/pnas.0905190107
37. Löhr H, Hess S, Pereira MMA, et al. Diet-induced growth is regulated via acquired leptin resistance and engages a Pomc-somatostatin-growth hormone circuit. *Cell Rep*. 2018;23(6):1728-1741. doi:10.1016/j.celrep.2018.04.018
38. Bartolomucci A, Possenti R, Levi A, Pavone F, Moles A. The role of the Vgf gene and VGF-derived peptides in nutrition and metabolism. *Genes Nutr*. 2007;2(2):169-180. doi:10.1007/s12263-007-0047-0

39. Nguyen AD, Mitchell NF, Lin S, et al. Y1 and Y5 receptors are both required for the regulation of food intake and energy homeostasis in mice. *PLoS One*. 2012;7(6):e40191. doi:10.1371/journal.pone.0040191
40. Qi Y, Lee NJ, Ip CK, et al. NPY derived from AGRP neurons controls feeding via Y1 and energy expenditure and food foraging behaviour via Y2 signalling. *Mol Metab*. 2022;59(May):101455. doi:10.1016/j.molmet.2022.101455
41. Vagena E, Crneta J, Engström P, et al. ASB4 modulates central Melanocortinergic neurons and calcitonin signaling to control satiety and glucose homeostasis. *Sci Signal*. 2022;15(733):eabj8204. doi:10.1126/scisignal.abj8204
42. Xiao C, Liu N, Province H, Piñol RA, Gavrilova O, Reitman ML. BRS3 in both MC4R- and SIM1-expressing neurons regulates energy homeostasis in mice. *Mol Metab*. 2020;36(June):100969. doi:10.1016/j.molmet.2020.02.012
43. Shi Z, Bonillas AC, Wong J, Padilla SL, Brooks VL. Neuropeptide Y suppresses Thermogenic and cardiovascular sympathetic nerve activity via Y1 receptors in the paraventricular nucleus and dorsomedial hypothalamus. *J Neuroendocrinol*. 2021;33(8):e13006. doi:10.1111/jne.13006
44. Sengul G, Watson C. Chapter 13 – spinal cord. In: Watson C, Paxinos G, Puelles L, eds. *The Mouse Nervous System*. Academic Press; 2012:424-458. doi:10.1016/B978-0-12-369497-3.10013-5
45. Abramova M, Calas A, Thibault J, Ugrumov M. Tyrosine hydroxylase in vasopressinergic axons of the pituitary posterior lobe of rats under salt-loading as a manifestation of neurochemical plasticity. *Neural Plast*. 2000;7(3):179-191. doi:10.1155/NP.2000.179
46. Romanov RA, Harkany T. Neuronal heterogeneity in the paraventricular nucleus of the hypothalamus as revealed by single-cell RNA-Seq. *Curr Opin Endocr Metab Res*. 2022;25(August):100366. doi:10.1016/j.coemr.2022.100366
47. Herbison AE. Sexually dimorphic expression of androgen receptor Immunoreactivity by somatostatin neurones in rat hypothalamic periventricular nucleus and bed nucleus of the stria terminalis. *J Neuroendocrinol*. 1995;7(7):543-553. doi:10.1111/j.1365-2826.1995.tb00791.x
48. Iacovazzo D, Caswell R, Bunce B, et al. Germline or somatic GPR101 duplication leads to X-linked acrogigantism: a clinico-pathological and genetic study. *Acta Neuropathol Commun*. 2016;4(1):56. doi:10.1186/s40478-016-0328-1
49. Carson KE, Alvarez J, Mackley JQ, Alberto Travagli R, Browning KN. Perinatal high-fat diet exposure alters oxytocin and Corticotropin releasing factor inputs onto vagal Neurocircuits controlling gastric motility. *J Physiol*. 2023;601(14):2853-2875. doi:10.1113/JP284726
50. Wolf FA, Angerer P, Theis FJ. SCANPY: large-scale single-cell gene expression data analysis. *Genome Biol*. 2018;19(1):15. doi:10.1186/s13059-017-1382-0
51. Traag VA, Waltman L, van Eck NJ. From Louvain to Leiden: guaranteeing well-connected communities. *Sci Rep*. 2019;9(1):5233. doi:10.1038/s41598-019-41695-z
52. Agrawal A, Ali A, Boyd S. Minimum-distortion embedding. *Found Trends Mach Learn*. 2021;14(3):211-378. doi:10.1561/2200000090
53. Verhaagen J, Hobo B, Ehlert EME, et al. Small scale production of recombinant adeno-associated viral vectors for gene delivery to the nervous system. In: Boon CJF, Wijnholds J, eds. *Retinal Gene Therapy: Methods and Protocols (Methods in Molecular Biology)*. Springer; 2018:3-17. doi:10.1007/978-1-4939-7522-8_1
54. Tervo DGR, Hwang B-Y, Viswanathan S, et al. A designer AAV variant permits efficient retrograde access to projection neurons. *Neuron*. 2016;92(2):372-382. doi:10.1016/j.neuron.2016.09.021
55. Challis RC, Kumar SR, Chan KY, et al. Systemic AAV vectors for widespread and targeted gene delivery in rodents. *Nat Protoc*. 2019;14(2):379-414. doi:10.1038/s41596-018-0097-3
56. R Core Team. *R: A Language and Environment for Statistical Computing*. R Foundation for Statistical Computing; 2021. https://www.R-project.org/

SUPPORTING INFORMATION

Additional supporting information can be found online in the Supporting Information section at the end of this article.

How to cite this article: Berkhout JB, Poormoghadam D, Yi C, Kalsbeek A, Meijer OC, Mahfouz A. An integrated single-cell RNA-seq atlas of the mouse hypothalamic paraventricular nucleus links transcriptomic and functional types. *J Neuroendocrinol*. 2024;36(2):e13367. doi:10.1111/jne.13367